Astronomy & Astrophysics manuscript no. output
July 3, 2019

On the existence of warm H-rich pulsating white dwarfs

Leandro G. Althaus[1,2], Alejandro H. Córsico[1,2], Murat Uzundag[3], Andrzej S. Baran[4], Maja Vučković[3], Leila M. Calcaferro[1,2], Keaton J. Bell[5], S. O. Kepler[6], Roberto Silvotti[7], Gerard Vauclair[8,9]

[1] Grupo de Evolución Estelar y Pulsaciones. Facultad de Ciencias Astronómicas y Geofísicas, Universidad Nacional de La Plata, Paseo del Bosque s/n, 1900 La Plata, Argentina
[2] IALP - CONICET
[3] Instituto de Física y Astronomía, Universidad de Valparaiso, Gran Bretaña 1111, Playa Ancha, Valparaíso 2360102, Chile
[4] Uniwersytet Pedagogiczny, Obserwatorium na Suhorze, ul. Podchorążych 2, 30-084 Kraków, Polska
[5] Max-Planck-Institut für Sonnensystemforschung (MPS), Justus-von-Liebig-Weg 3, 37077 Göttingen, Germany
[6] Instituto de Física, Universidade Federal do Rio Grande do Sul, 91501-900, Porto-Alegre, RS, Brazil
[7] INAF – Osservatorio Astrofisico di Torino, strada dell'Osservatorio 20, 10025 Pino Torinese, Italy
[8] Université de Toulouse; UPS-OMP; IRAP; Toulouse, France
[9] CNRS; IRAP; 14 av. Edouard Belin, F-31400 Toulouse, France

Received ; accepted

ABSTRACT

Context. The possible existence of warm ($T_{\rm eff} \sim 19\,000$ K) pulsating DA white dwarf (WD) stars, hotter than ZZ Ceti stars, was predicted in theoretical studies more than 30 yr ago. These studies reported the occurrence of g-mode pulsational instabilities due to the κ mechanism acting in the partial ionization zone of He below the H envelope in models of DA WDs with very thin H envelopes ($M_{\rm H}/M_\star \lesssim 10^{-10}$). However, to date, no pulsating warm DA WD has been discovered, despite the varied theoretical and observational evidence suggesting that a fraction of WDs should be formed with a range of very low H content.
Aims. Here, we re-examine the pulsational predictions for such WDs on the basis of new full evolutionary sequences. We analyze all the warm DAs observed by TESS satellite up to Sector 9 in order to search for the possible pulsational signal.
Methods. We compute WD evolutionary sequences of masses 0.58 and 0.80 $M_\odot$ with H content in the range $-14.5 \lesssim \log(M_{\rm H}/M_\star) \lesssim -10$, appropriate for the study of pulsational instability of warm DA WDs. Initial models were extracted from progenitors that were evolved through very late thermal pulses on the early cooling branch. We use LPCODE stellar code to which we have incorporated a new full-implicit treatment of time-dependent element diffusion for precisely modeling the H/He transition zone in evolving WD models with very low H content. The non-adiabatic pulsations of our warm DA WD models were computed in the effective temperature range of 30 000 − 10 000 K, focusing on $\ell = 1$ g modes with periods in the range 50 − 1500 s.
Results. We find that traces of H surviving the very late thermal pulse float to the surface, eventually forming thin pure H envelopes and rather extended H/He transition zones. We find that such extended transition zones inhibit the excitation of g modes due to partial ionization of He below the H envelope. Only in the case that the H/He transition is assumed much more abrupt than predicted by time-dependent diffusion, models do exhibit pulsational instability. In this case, instabilities are found only in WD models with H envelopes in the range of $-14.5 \lesssim \log(M_{\rm H}/M_\star) \lesssim -10$ and at effective temperatures higher than those typical of ZZ Ceti stars, in agreement with previous studies. None of the 36 warm DAs observed so far by TESS satellite are found to pulsate.
Conclusions. Our study suggests that the non-detection of pulsating warm DAs, if WDs with very thin H envelopes do exist, could be attributed to the presence of a smooth and extended H/He transition zone. This could be considered as an indirect proof that element diffusion indeed operates in the interior of WDs.

Key words. stars: evolution — stars: interiors — stars: white dwarfs

1. Introduction

The existence of various types of pulsating white dwarf (WD) stars characterized by multiperiodic luminosity variations due to g(gravity)-mode pulsations has been well established by theoretical and observational evidence (Winget & Kepler 2008; Fontaine & Brassard 2008; Althaus et al. 2010b). During their lives, WDs experience at least one stage of pulsational instability, during which peak-to-peak amplitudes between 0.1 mmag and 0.4 mag in typical optical light curves are expected. Among the different types of observed pulsating WDs (see Córsico et al. 2019, submitted) we mention the most abundant ones: *(i)* the hydrogen (H)-rich variables ZZ Ceti or DAVs (Landolt 1968) at low effective temperatures and high gravities ($10\,400$ K $\lesssim T_{\rm eff} \lesssim 12\,400$ K and $7.5 \lesssim \log g \lesssim 9.1$); *(ii)* the variables V777 Her or DBVs, with almost pure helium (He) atmospheres, spanning a range in effective temperature and surface gravity of $22\,400$ K $\lesssim T_{\rm eff} \lesssim 32\,000$ K and $7.5 \lesssim \log g \lesssim 8.3$, theoretically predicted by Winget et al. (1982b) before their discovery (Winget et al. 1982a); *(iii)* the "hot DAVs" ($T_{\rm eff} \sim 30\,000$ K, $7.3 \lesssim \log g \lesssim 7.8$; Kurtz et al. 2008, 2013), whose existence was anticipated by the theoretical calculations of Shibahashi (2005, 2007); *(iv)* the pulsating PG1159 stars or GW Vir variable stars, after the prototype of the class, PG 1159−035 (McGraw et al. 1979), rich in He, carbon (C), and oxygen (O), being the hottest known class of pulsating WDs and pre-WDs ($80\,000$ K $\lesssim T_{\rm eff} \lesssim 180\,000$ K and $5.5 \lesssim \log g \lesssim 7.5$); and *(v)* the H-rich ELMVs (Extremely Low-Mass WDs variable) with $7\,800$ K $\lesssim T_{\rm eff} \lesssim 10\,000$ K and $6 \lesssim \log g \lesssim 6.8$ (Hermes et al. 2012) and the He/H-atmosphere

pre-ELMVs (8 000 K $\lesssim T_{\rm eff} \lesssim$ 13 000 K and $4 \lesssim \log g \lesssim 5$), the probable precursors of ELMVs (Maxted et al. 2013).

In addition to these pulsating WDs, early theoretical calculations predicted the existence of pulsating DA WDs hotter than ZZ Ceti stars, hereinafter warm DAVs, expected to be found at effective temperatures comparable to those of the cool edge of the DBV instability strip. In fact, theoretical investigations carried out by Winget et al. (1982b) (see, also, Winget 1982) led to the discovery of g-mode pulsational instability due to $\kappa-$mechanism operating in the partial ionization zone of He below the H envelope in models of DA WDs harboring very thin H envelopes ($M_{\rm H}/M_\star \lesssim 10^{-10}$), for effective temperatures of $\sim$ 19 000 K. A major issue of this finding was related to the possibility of constraining the mass of the residual H envelope left in a WD by eventually observing pulsating WDs near this temperature (Winget et al. 1982b).

The existence of WDs with such very thin H envelopes is not discarded neither by the theory of stellar evolution nor by observations. From the observational point of view, nearly 80% of the spectroscopically identified WDs are characterized by H-rich atmospheres. Systematic spectroscopic and asteroseismological studies indicate that between 15% and 20% of such WDs are expected to harbor thin H envelopes with $M_{\rm H} \lesssim 10^{-6} M_\odot$ (see Tremblay & Bergeron 2008; Castanheira & Kepler 2009; Romero et al. 2012). On the other hand, single stellar evolution theory predicts that usually WDs should be formed with a total H content of about $M_{\rm H} \sim 10^{-3} - 10^{-5} M_\odot$, depending on the stellar mass and metallicity of the progenitor (Althaus et al. 2015). However, certain evolutionary scenarios predict the formation of DA WDs with thin H envelopes. One of such scenarios involves the occurrence of very late thermal pulses (VLTP) that take place when the WD progenitor experiences its last thermal pulse on the early WD cooling branch. In this case, the H-rich envelope is ingested by the He-shell flash convective zone, where H is burnt in the hot interior of the star (Iben & MacDonald 1995; Herwig et al. 1999). Recent full evolutionary calculations of the event by Miller Bertolami et al. (2017) predict the formation of DA WDs with H content of $M_{\rm H} \lesssim 10^{-7} M_\odot$. In line with this, if the last thermal pulse happens during the horizontal evolution of the post-AGB star in the HR diagram, a scenario termed Late Thermal Pulse (LTP) occurs (Blöcker 2001). Then, the H-rich envelope is not burned but diluted by the deepening of the convective envelope once the star evolves back to the AGB after the LTP. As shown by Althaus et al. (2005a), the H diluted into the deeper parts of the envelope is later burned as the H-deficient star contracts again to the WD cooling track, leading to the formation of WDs with a low H-content ($M_{\rm H} \lesssim 10^{-6} - 10^{-7} M_\odot$). For the case of VLTP remnants of masses $M_{\rm WD} \gtrsim 0.6 M_\odot$, Miller Bertolami et al. (2017) obtained DA WDs with H content of the order of $10^{-11} M_\odot$. On the other hand, the existence of WDs with extremely thin H envelopes (of the order of $M_{\rm H} \lesssim 10^{-14} M_\odot$) has been invoked in the context of the spectral evolution that some WDs experience as they evolve, see Fontaine & Wesemael (1987); Shibahashi (2007). Finally, additional observational evidence supporting the picture that a fraction of DA WDs could harbour thin H envelopes is provided by a new dynamical mass determination of WD 40 Eri B, for which a fractional H envelope mass of $\approx 10^{-10}$ has recently been inferred by Bond et al. (2017) (see, also, Romero et al. 2019). All this evidence suggests that WDs could be formed with H envelopes orders of magnitude less massive than the canonical value of $M_{\rm H} \approx 10^{-4} M_\odot$.

In view of these considerations, and despite the numerous discoveries of pulsating WD stars in the last decade, both from the ground and from space, it is surprising that no warm DAV WD has been detected thus far. Ground-based observations, particularly carried out with the spectral observations of the Sloan Digital Sky Survey (SDSS; York et al. 2000), have increased the number of known WDs by a factor of 15 (Kleinman et al. 2013; Kepler et al. 2016, 2019; Kepler & Romero 2017; Gentile Fusillo et al. 2019) and the number of pulsators by a factor of 4 (Mukadam et al. 2004; Mullally et al. 2005; Castanheira et al. 2006; Voss et al. 2007; Nitta et al. 2009; Castanheira et al. 2013). On the other hand, the *Kepler* satellite observations, both main mission (Borucki et al. 2010) and K2 (two-wheel operation, Howell et al. 2014), increased the number of known WD pulsators by a factor of 2 (Hermes et al. 2017). The fact that no warm DAV has emerged from the various surveys has prompted us to re-examine the pulsational properties of warm DAV WDs on the basis of detailed WD evolutionary sequences that incorporate a full implicit treatment of time-dependent element diffusion, appropriate for modeling the formation of the H-rich envelope and H/He transition in WDs with very thin H envelopes resulting from post-VLTP remnants. In this study, we also examine the pulsational spectra provided by TESS satellite (Ricker et al., 2015) to search for possible candidates of warm DAV WDs.

The paper is organized as follows. In Sect. 2 we present null results in the search for warm DAVs on the basis of a sample of DA WDs with effective temperatures between $\sim$ 17 500 K and $\sim$ 22 500 K observed with TESS. In Sect. 3 we briefly describe some details of our stellar and pulsational codes, and evolutionary sequences, and present in detail our treatment of time-dependent element diffusion. In Sect. 4 we present the predictions of our evolution and pulsation analyses. Finally, in Sect. 5 we summarize the main findings of the paper, and we elaborate on our conclusions.

2. Observational insights from TESS

We have searched for pulsations in warm DA WDs observed by the recent NASA Space Mission of Transiting Exoplanet Survey Satellite (TESS; Ricker et al. 2014). To this end, we have cross-checked the targets from the Montreal White Dwarf Database (MWDD)[1] (Dufour et al. 2017), which provides information about all known WDs, with the targets observed with TESS. We found 36 objects matching our criteria of $T_{\rm eff}$ between 17 500 and 22 500 K. They are listed in Table A.1 of the Appendix A[2].

We used the short-cadence (SC) observations sampled every 2 minutes, which allows us to analyze the frequency range up to the Nyquist frequency at 4200 μHz. We downloaded all available data (sector 1 to 9) from the "Barbara A. Mikulski Archive for Space Telescopes" (MAST)[3]. The data are in the FITS format which includes all the photometric information, which have been already processed with the Pre-Search Data Conditioning Pipeline (Jenkins et al. 2016) to remove common instrumental trends. From the FITS file, first we have extracted times in barycentric corrected Julian days ("BJD - 245700"), and fluxes ("PDCSAP FLUX"). In order to increase the signal-to-noise ratio (S/N) of the data in the Fourier space, we detrended the light curves after σ clipping , removing the outliers that vary significantly from the local standard deviation (σ) by applying a running 4σ clipping mask. The fluxes were then normalized and transformed to amplitudes in parts-per-thousand (ppt) unit ($(\Delta I/I - 1) \times 1000$).

[1] http://www.montrealwhitedwarfdatabase.org

[2] We note that stars fainter than $T_{\rm mag} = 17$ have detection thresholds not useful for detecting pulsations.

[3] http://archive.stsci.edu

In order to search for periodicity, we assessed the Fourier Spectrum of each light curve. Then, we calculated the median noise level of each data set (σ) and used 5σ as the detection threshold (Baran et al. 2015). The amplitude spectra of all DA WDs analyzed are presented in Figs. A.1 to A.6, where the blue line represents the 5σ threshold. As can be seen, none of the 36 DA WDs depicted in Figs. A.1 to A.6 have any signal above the threshold in the frequency region of interest. Therefore, we conclude that the sample of DA WDs observed with TESS does not show any signs of pulsations up to the Nyquist frequency at 4200 μHz.

3. Evolutionary/pulsational models and numerical inputs

Our pulsation calculations are based on full WD evolutionary models of different stellar masses. Initial models were extracted from progenitor star models that were evolved from the ZAMS, to the thermally-pulsing AGB phase, and through the VLTP occurring at the beginning of the cooling branch, Miller Bertolami & Althaus (2006). VLTP is one of the most plausible single-evolution scenarios that predicts the formation of hydrogen-poor WDs, see Córsico et al. 2019 for recent discussion. To encompass the range of H envelope mass that should be expected in warm DAV WDs, the H content of our post VLTP sequence has been artificially reduced, mimicking a more efficient hydrogen mixing and burning during the VLTP. Specifically, we concentrate on warm DAV WD models of masses 0.58 and $0.80 M_{\odot}$ with H content in the range $-14.5 \lesssim \log(M_{\rm H}/M_{\star}) \lesssim -10$.

We use our stellar evolutionary code, LPCODE, to follow the evolution of our selected post-VLTP remnants from the very early stages of WD evolution down to an effective temperature of 10,000K, well below the expected domain of warm DAV WDs. LPCODE is a well tested and calibrated stellar code; see Althaus et al. (2003), Althaus et al. (2005b), Althaus et al. (2015), and Miller Bertolami (2016) for details. LPCODE has been widely used to study the evolution of low-mass and WD stars — see Miller Bertolami et al. (2008), García-Berro et al. (2010), Althaus et al. (2010a), Renedo et al. (2010), Miller Bertolami et al. (2011), Wachlin et al. (2011), Córsico et al. (2012), Althaus et al. (2013), and Miller Bertolami (2016).

We compute the non-adiabatic pulsations of our warm DA WD models in the effective-temperature range 30,000 K – 10,000 K, amply covering the region where warm DAV WDs should be expected. We have focused on $\ell = 1$ g modes with periods in the range 50 – 1500 s. To this end, we employ the non-adiabatic version of the LP-PUL pulsation code, which is described in Córsico et al. (2006).

3.1. Numerical treatment of time-dependent element diffusion

After the violent proton burning and mixing during the VLTP episode, only tiny vestiges of H remain, extending from the surface down to as deep as $3 \times 10^{-4} M_{\odot}$. As WD evolves along the cooling branch, such traces of H will float to the surface as a result of gravitational settling, thus forming an increasing pure (and thin) H envelope. The thickness of the resulting H envelope and the shape of the H/He interface are a key issue, because to what extent the inner tail of H distribution penetrates into the pure He buffer will determine the pulsational stability properties of the stellar models. Given the characteristic diffusion time scales involved, a time-dependent treatment of element diffusion becomes necessary. We have explored two situations: a discontinuous H/He transition separating the pure H envelope from the underlying pure He buffer, and a H/He interface as predicted by element diffusion.

Under the influence of gravity, partial pressure, and induced electric fields, the diffusion velocities in a multicomponent plasma satisfy the set of $N-1$ independent equations (Burgers 1969)[4]:

$$\frac{dp_i}{dr} - \frac{\varrho_i}{\varrho}\frac{dp}{dr} - n_i Z_i e E = \sum_{j\neq i}^{N} K_{ij}\left(w_j - w_i\right), \tag{1}$$

where, p_i, ϱ_i, n_i, Z_i, and w_i denote, respectively, the partial pressure, mass density, number density, mean charge, and diffusion velocity for chemical species i. N is the number of ionic species plus electrons. The unknown variables are w_i and the electric field E. Resistance coefficients K_{ij} are from Paquette et al. (1986). This set of equations is solved together with the equations for no net mass flow $\sum_i A_i n_i w_i = 0$ and no electrical current $\sum_i Z_i n_i w_i = 0$.

Following Iben & MacDonald (1985), Eq. (1) can be rearranged to obtain (for the ions)

$$\frac{1}{n_i}\sum_{j\neq i}^{N} K_{ij}\left(w_i - w_j\right) - Z_i e E = \alpha_i - k_{\rm B} T \frac{d\ln n_i}{dr}, \tag{2}$$

where $\alpha_i = -A_i\, m_{\rm H}\, g - k_{\rm B}\, T\, (d\ln T/dr)$, being g the gravitational acceleration. w_i can be written

$$w_i = w_i^{\rm gt} - \sum_j \sigma_{ij}\frac{d\ln n_j}{dr}, \tag{3}$$

where $w_i^{\rm gt}$ stands for the velocity component due to gravity and temperature gradient (gravitational settling component). The components due to gradients in number density are referred to as chemical diffusion components. The summation is done *for the ions only*. This equation, together with the conditions for no net mass flow and electrical current, can be solved using matrix inversion to find $w_i^{\rm gt}$ and σ_{ij}, which finally are employed to follow the evolution of the number density of ionic species i

$$\frac{\partial n_i}{\partial t} = -\frac{1}{r^2}\frac{\partial}{\partial r}\left(r^2\, n_i\, w_i\right). \tag{4}$$

For numerical purposes, we write this equation in terms of the abundance by mass X_i of species i, given by $X_i = \varrho_i/\varrho$

$$\varrho\,\frac{\partial X_i}{\partial t} = -\frac{1}{r^2}\frac{\partial}{\partial r}\left(r^2\, X_i\, \varrho\, w_i\right). \tag{5}$$

We multiply this equation by $4\pi r^2$ and integrate over the radial coordinate r from $r - \Delta r/2$ to $r + \Delta r/2$, to obtain

$$\Delta m \left.\frac{\partial X_i}{\partial t}\right|_r = -\left(4\pi\varrho r^2 X_i w_i\right)\Big|_{r-\Delta r/2}^{r+\Delta r/2}, \tag{6}$$

[4] We neglect thermal diffusion which is not relevant in WDs (Iben & MacDonald 1985).

where $\Delta m = \int_{r-\Delta r/2}^{r+\Delta r/2} 4\pi r^2 \varrho dr$ (we assume Δr small enough for $\partial X_i/\partial t$ to be constant over Δr). Eq. (6) simply states that the difference of flux of mass of element i between the two borders of a spherical shell is equal to the time variation of the mass of element i in the shell. We discretize this equation with respect to time and space by dividing the star into K mesh points, with the lagrangian mass coordinate of the k^{th} mesh point being m_k (the mass inside the sphere of radius r_k). In what follows, all the quantities with an indice k are evaluated at the mesh point k. The mesh points are numbered from 1 at the surface to K at the centre. The mass of element i removed from mesh point $k+1$ and added to mesh point k per unit time becomes:

$$4\pi r_{k+1/2}^2 \varrho_{k+1/2} (X_i w_i)_{k+1/2}, \tag{7}$$

where the subscript $k+1/2$ means that quantities are evaluated at the midpoint between the mesh points $k+1$ and k. For instance, $r_{k+1/2} = (r_k + r_{k+1})/2$. We have a similar expression for the mass of element i removed from mesh point k and added to mesh point $k-1$. Denoting with $X_{i,k}$ the abundance by mass of element i evaluated at the mesh point k and considering that $\Delta m_k = \int_{r_{k+1/2}}^{r_{k-1/2}} 4\pi r^2 \varrho dr$, we have

$$\Delta m_k \frac{\partial (X_{i,k})}{\partial t} = 4\pi r_{k+1/2}^2 \, \varrho_{k+1/2} \, (X_i w_i)_{k+1/2} - 4\pi r_{k-1/2}^2 \, \varrho_{k-1/2} \, (X_i w_i)_{k-1/2}. \tag{8}$$

The left hand term of this equation is discretized as

$$\Delta m_k \frac{X_{i,k} - X_{i,k}^0}{\Delta t}, \tag{9}$$

where $X_{i,k}^0$ corresponds to the abundance by mass of element i at mesh point k evaluated at the beginning of time step Δt, and $X_{i,k}$ the abundance of the same element at k at the end of the time step. Note that we are considering the average of the product $X_i \, w_i$ (specifically, $X_i \, w_i^{\rm gt}$ and $X_i \, \sigma_{ij}$) between two adjacent mesh points and not the product of the averages of X_i and w_i. In this way, mass conservation is guaranteed in Eq.8, as we imposed the condition of no net mass flow at each mesh point k at calculating the diffusion velocities[5].

Taking $\Delta m_k = \varrho_k \, \Delta V_k$, with $\Delta V_k = 4\pi(r_{k-1/2}^3 - r_{k+1/2}^3)/3$ we obtain

$$X_{i,k} - X_{i,k}^0 = \frac{\Delta t}{\varrho_k \, \Delta V_k} \, 4\pi r_{k+1/2}^2 \, \varrho_{k+1/2} \, (X_i w_i)_{k+1/2} - \frac{\Delta t}{\varrho_k \, \Delta V_k} \, 4\pi r_{k-1/2}^2 \, \varrho_{k-1/2} \, (X_i w_i)_{k-1/2}, \tag{10}$$

where (from Eq. 3)

$$(X_i w_i)_{k+1/2} = \frac{X_{i,k} w_{i,k}^{\rm gt} + X_{i,k+1} w_{i,k+1}^{\rm gt}}{2} - \sum_j \frac{\sigma_{ij,k} X_{i,k} + \sigma_{ij,k+1} X_{i,k+1}}{2} \frac{2}{X_{j,k} + X_{j,k+1}} \frac{\varrho_k X_{j,k} - \varrho_{k+1} X_{j,k+1}}{\varrho_{k+1/2}(r_k - r_{k+1})} \tag{11}$$

and

$$(X_i w_i)_{k-1/2} = \frac{X_{i,k} w_{i,k}^{\rm gt} + X_{i,k-1} w_{i,k-1}^{\rm gt}}{2} - \sum_j \frac{\sigma_{ij,k} X_{i,k} + \sigma_{ij,k-1} X_{i,k-1}}{2} \frac{2}{X_{j,k} + X_{j,k-1}} \frac{\varrho_{k-1} X_{j,k-1} - \varrho_k X_{j,k}}{\varrho_{k-1/2}(r_{k-1} - r_k)} \tag{12}$$

We have a set of difference equations at each mesh point k, the solution of which will give us $X_{i,k}$ for all species i at each k. The boundary conditions at the center, $k = K$, and at the surface, $k = 1$, are respectively

$$\Delta m_K \frac{\partial (X_{i,K})}{\partial t} = -4\pi r_{K-1/2}^2 \varrho_{K-1/2} (X_i w_i)_{K-1/2} \tag{13}$$

$$\Delta m_1 \frac{\partial (X_{i,1})}{\partial t} = 4\pi r_{1+1/2}^2 \varrho_{1+1/2} (X_i w_i)_{1+1/2}, \tag{14}$$

for which we proceed as above. Eqs. (10) to (14) can be written in a compact form as

$$\begin{cases} B_i(\mathbf{X}_{\rm k}, \mathbf{X}_{\rm k+1}) = 0 & k = 1 \\ G_{i,k}(\mathbf{X}_{\rm k-1}, \mathbf{X}_{\rm k}, \mathbf{X}_{\rm k+1}) = 0 & 2 \le k \le K-1 \\ C_i(\mathbf{X}_{\rm k-1}, \mathbf{X}_{\rm k}) = 0 & k = K \end{cases} \tag{15}$$

where $\mathbf{X}_{\rm k}$ means $X_{i,k}\,\{i{=}1, \cdots, N_{\rm ions}\}$ with $N_{\rm ions}$ the number of species i. To solve this set of non-linear equations we use an iterative full implict method, in which an initial solution is gradually improved by applying successive simultaneous corrections to all variables at all mesh points. Implicit methods, in constrast with semi-implicit methods, are usually preferred because of the superior stability characteristics. In addition, they maintain the sum of X_i almost constant over large time integrations. This is a relevant issue, since in this work we are interested in the formation and evolution of H envelopes less massive than $10^{-10} M_\odot$. The treatment present here is an improvement over that presented in Althaus et al. (2003), based on the semi-implicit method described in Iben & MacDonald (1985).

Let $\mathbf{X}^1$ be a first approximation to the set of Eqs. 15, which as a firts guess we take it as the solution at the previous time $t - \Delta t$. Clearly, since this is only an approximation to the solution, then $B_i(1) \neq 0$, $G_{i,k}(1) \neq 0$, and $C_i(1) \neq 0$. Let $\delta\mathbf{X}$ the corresponding corrections to all variables at all mesh points; we get a second approximation $\mathbf{X}^2 = \mathbf{X}^1 + \delta\mathbf{X}$, so that now $B_i(2) = 0$, $G_{i,k}(2) = 0$, and $C_i(2) = 0$. If corrections are small, a first-order Taylor expansion leads

$$\sum_j \frac{\partial G_{i,k}}{\partial X_{j,k-1}} \delta X_{j,k-1} + \sum_j \frac{\partial G_{i,k}}{\partial X_{j,k}} \delta X_{j,k} + \sum_j \frac{\partial G_{i,k}}{\partial X_{j,k+1}} \delta X_{j,k+1} = -G_{i,k}(1) \tag{16}$$

[5] For instance,

$$\sum_i (X_i w_i)_{k+1/2} = \sum_i \frac{X_{i,k} w_{i,k} + X_{i,k+1} w_{i,k+1}}{2} \propto \underbrace{\sum_i A_i n_{i,k} w_{i,k}}_{=0} + \underbrace{\sum_i A_i n_{i,k+1} w_{i,k+1}}_{=0} = 0$$

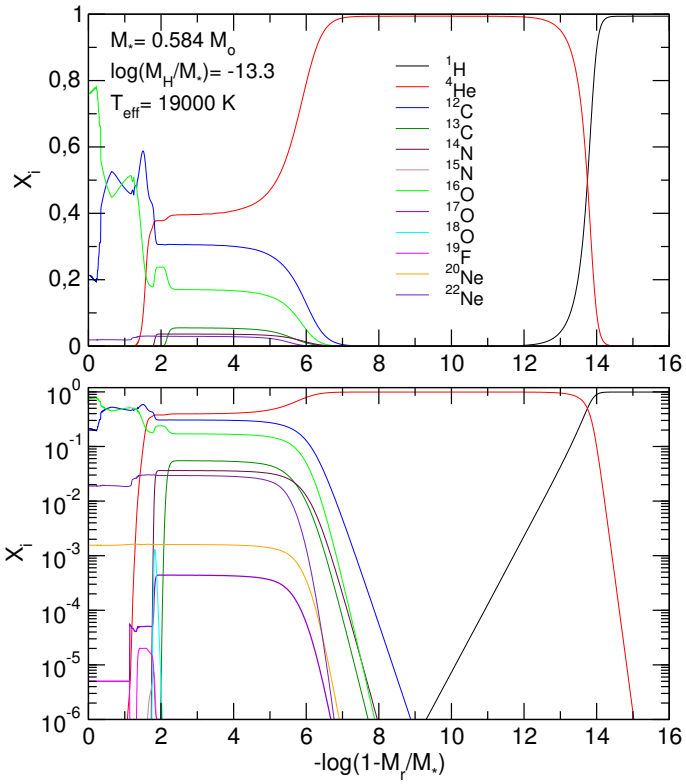

Fig. 1. Upper panel: fractional abundance by mass of selected nuclear species in terms of the outer mass fraction, corresponding to a DA WD model characterized by $M_\star$=0.584$M_\odot$, $T_{\rm eff}$=19 000 K and $\log(M_{\rm H}/M_\star)$= −13.3. Lower panel: same as in the upper panel, but with a logarithmic scale for the chemical abundances.

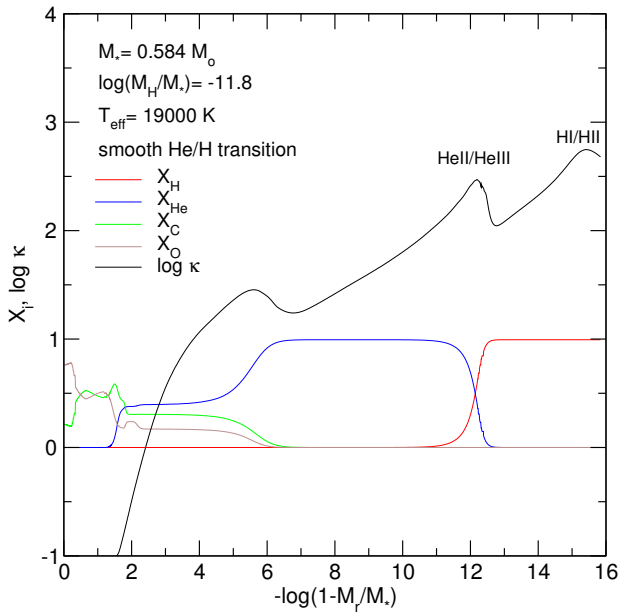

Fig. 2. Inner chemical profiles of ^{16}O, ^{12}C, ^{4}He and H, and the logarithm of the Rosseland opacity (κ) versus the outer mass fraction coordinate, corresponding to a DA WD model with $M_\star$=0.584$M_\odot$, $\log(M_{\rm H}/M_\star)$=−11.8, and $T_{\rm eff}$=19 000 K. The H/He interface is shaped by time-dependent element diffusion. The bumps in κ due to the second ionization of He and the ionization of H are evident.

and similarly for B_i and C_i. The derivatives are assessed at the first approximation. From here, the corrections $\delta\mathbf{X}$ are found by inverting a band-type matrix with non-vanishing coefficients only in blocks near the diagonal (because difference equations depend only on variables at adjacent points), by following the elimination procedure of Henyey et al. (1964). After several iterations (diffusion velocities are re-calculated at each iteration), the approximate solution is improved until the absolute value of all corrections drops below a given limit or the difference equations are satisfied to a given accuracy.

This implicit procedure for solving the time-dependent diffusion equations is efficient and stable. In particular, for our sequences with $M_{\rm H} = 10^{-11} M_\odot$, the total mass of the H content changes by less than 0.01% after 10^8 yr of evolution. After the convergence of a stellar model, the chemical abundance change due to element diffusion and convection (and nuclear reactions if any) for the next evolutionary time step is evaluated, and then the next stellar model is computed by solving the full set of stellar structure and evolution equations.

As an illustrative example of the performance of our new treatment of time-dependent element diffusion, in Fig. 1 we show the abundances by mass (X_i) of selected chemical species in terms of the external fractional mass, for a DA WD model with $M_\star$=0.584$M_\odot$, $T_{\rm eff}$=19 000 K and $\log(M_{\rm H}/M_\star)$=−13.3. The upper panel shows the abundances on a linear scale, thus emphasizing the dominant species, while the lower panel shows the abundances on a logarithmic scale, making it possible to clearly visualize the less abundant species. Note the tail of H digging into deeper layers. Element diffusion predicts a wide and smooth H/He transition zone. The imprints on the chemical abundance

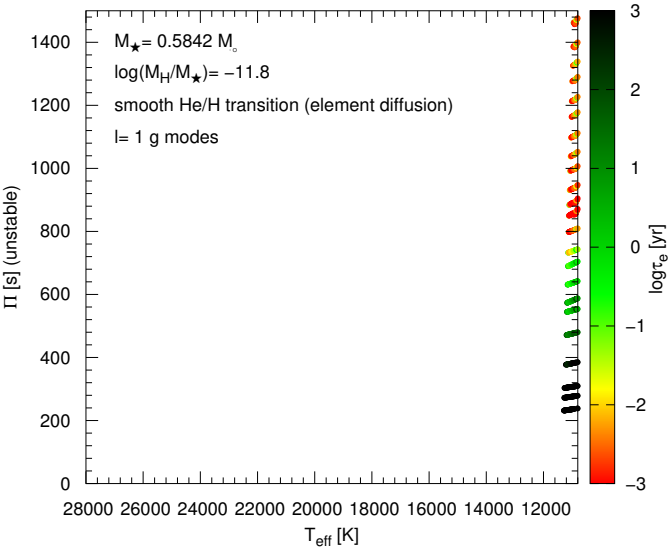

Fig. 3. Unstable ℓ=1 g-mode periods (Π) in terms of the effective temperature for the sequence of DA WD models with $M_\star$=0.584$M_\odot$ and $\log(M_{\rm H}/M_\star)$=−11.8. The H/He interface is shaped by time-dependent element diffusion (see Fig. 2). Color coding indicates the value of the logarithm of the e-folding time ($\tau_{\rm e}$) of each unstable mode (right scale). Only unstable modes for effective temperatures characteristic of the ZZ Ceti stage ($T_{\rm eff} \lesssim$ 11 500 K) are found.

distribution left by the violent H burning during VLTP are visible, in particular the high abundance of ^{13}C. Note also the presence of a thick intershell rich in He and carbon, left by the convection zone driven by the last He thermal pulses.

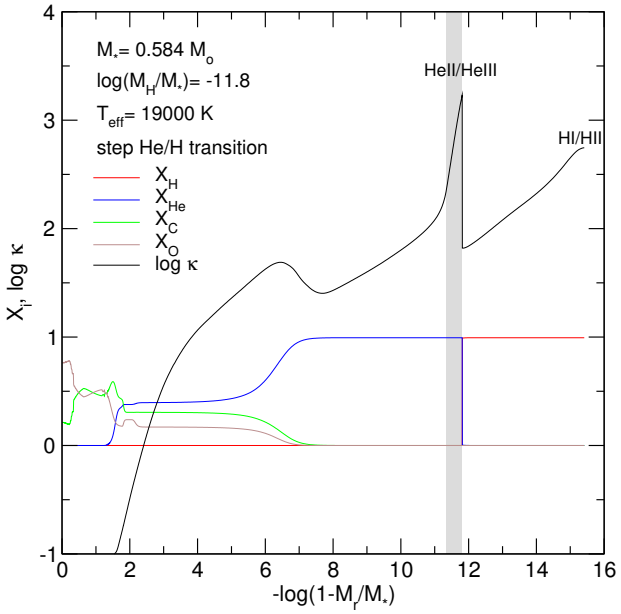

Fig. 4. Same as Fig. 2, but for the extreme case in which the H/He interface is assumed to be discontinuous (step-like shape). The vertical gray strip marks the convection zone driven by the 2nd ionization of He.

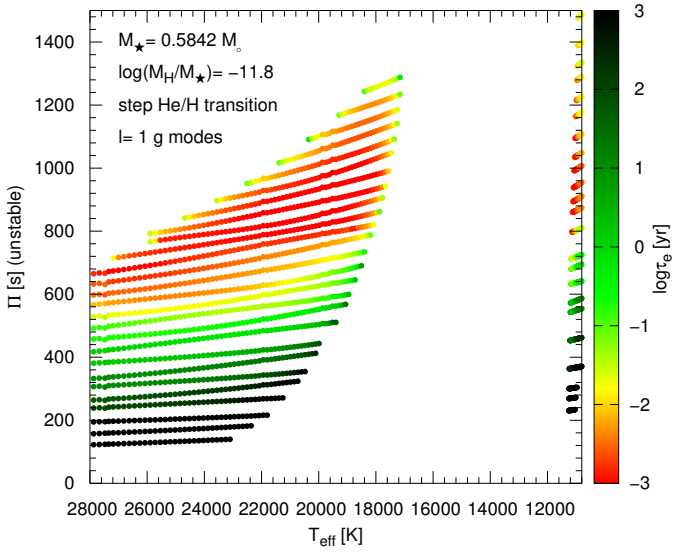

Fig. 5. Same as Fig. 3, but for the case in which the H/He interface has a step-like shape (see Fig. 4). Here, g modes with a wide range of periods are excited at high effective temperatures.

4. Evolutionary and pulsational results

In Fig. 2 we depict the chemical profiles of ^{16}O, ^{12}C, ^{4}He, H, and the Rosseland opacity as a function of the coordinate $-\log(1 - M_r/M_\star)$ for a template model with $M_\star$=0.584$M_\odot$, $\log(M_{\rm H}/M_\star)$=−11.8, and $T_{\rm eff}$=19 000 K. As in the situation analysed in Fig. 1, we also find that element diffusion leads to an extended H/He transition region, with the tail of the H profile reaching layers well below the point at which $X_{\rm He}$=$X_{\rm H}$=0.5. Note the presence of bumps in the Rosseland opacity corresponding to the second ionization of He ($\log T \sim 5.3$) and the ionization of H ($\log T \sim 4.58$). In particular, the HeII/HeIII bump is quite pronounced (note that what is shown is the logarithm of κ); however, it is unable to generate a convective zone. In Fig. 3 we depict the periods of unstable ℓ=1 modes versus $T_{\rm eff}$ corresponding to the same sequence of WD models ($M_\star$=0.584$M_\odot$, $\log(M_{\rm H}/M_\star)$=−11.8). Also shown is the e-folding time (in yr) of each unstable mode, which is defined as $\tau_{\rm e} = 1/|\Im(\sigma)|$, $\Im(\sigma)$, being σ the imaginary part of the complex eigenfrequency. It is an estimate of the time it would take a given mode to reach amplitudes large enough as to be observable. The e-folding time has to be compared with the evolutionary timescale ($\tau_{\rm evol}$), that represents the time that the WD spends evolving in the regime of interest. Notably, our results indicate that all g modes are pulsationally stable at high effective temperatures, so they do not appear in the plot. As the model cools, g modes become unstable due to the κ mechanism acting at the partial ionization zone of H for effective temperatures lower than $\sim$ 11 500 K, at the instability domain of the ZZ Ceti stars. We conclude that, when the H/He interface is shaped by element diffusion, there is no excitation of g modes at high effective temperatures due to the partial ionization of He.

In Fig. 4, we display the chemical profiles and the Rosseland opacity for the same WD model, but in this case the H/He transition region is not modeled by element diffusion, but it is assumed to have a step-like shape. Here, opacity exhibits a sharp peak at the region of the H/He chemical interface, thus resulting in the formation of a narrow convection zone (marked as a gray vertical strip in the figure) immediately below the H/He chemical interface. The peak in κ is due to the absence of H below the chemical transition of H/He. Indeed, the presence of H in this chemical transition when the interface is wide (Fig. 2), strongly reduces the total opacity. Hence, when H is absent, the opacity locally reaches much higher values (Fig. 4). Fig. 5 shows the period range of excited dipole modes in terms of the effective temperature for models with step-like shape H/He interface. At variance with the case depicted in Fig. 3, here we find g modes with a wide range of periods excited in a broad interval of high effective temperatures (50 000 K $\gtrsim T_{\rm eff} \gtrsim$ 17 000 K), apart from g modes excited at low temperatures in the ZZ Ceti domain. In addition, for most of the excited modes (specifically, for $\Pi \gtrsim 200$ s) the inequality $\tau_{\rm e} \ll \tau_{\rm evol}$ is satisfied, which ensures that the modes could reach observable amplitudes as the models are slowly evolving in that range of effective temperatures.

Our results confirm the early findings of Winget et al. (1982b) that in DA WD models with very thin H envelopes, $\log(M_{\rm H}/M_\star) \leq -10$, He is able to drive g-mode pulsations at effective temperatures $T_{\rm eff} \sim$ 19 000 K. Two other relevant works carried out almost at the same time as the analysis by Winget et al. (1982b), that is, the studies by Dolez & Vauclair (1981) and Dziembowski & Koester (1981), reported pulsational instability due to the κ mechanism acting at the partial ionization region of the He in models with very thin H envelopes. Nevertheless, the pulsational instabilities they found appear at lower effective temperatures ($T_{\rm eff} \lesssim$ 13500 K), compatible with the instability strip of ZZ Ceti stars.

Fig. 6 illustrates the case of a sequence of models with $M_\star$ = 0.584$M_\odot$ but with a thinner H envelope of $\log(M_{\rm H}/M_\star) = -12.8$, assuming a step-like shaped H/He transition region. The results are qualitatively similar to the case displayed in Fig. 5 for $\log(M_{\rm H}/M_\star) = -11.8$, that is, g modes are driven by the κ mechanism due to the partial ionization of He for effective temperatures higher than those characterizing ZZ Ceti stars. We have also analyzed the case in which these models harbor a smooth H/He interface modeled by time-dependent element diffusion. Again, in this case, we do not find unstable modes at high effective temperatures. We also explored the predictions of an even

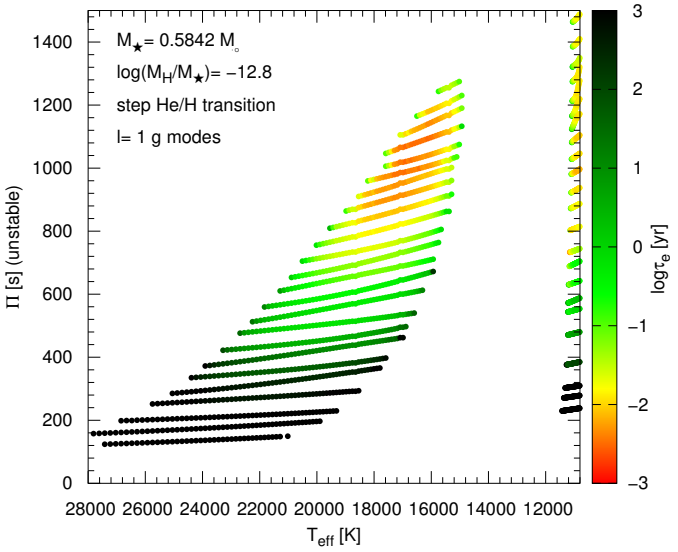

Fig. 6. Same as Fig. 5 but for $\log(M_{\rm H}/M_\star) = -12.8$. Again, in this case, a lot of g modes are excited at high effective temperatures, apart from the excited modes at the ZZ Ceti phase.

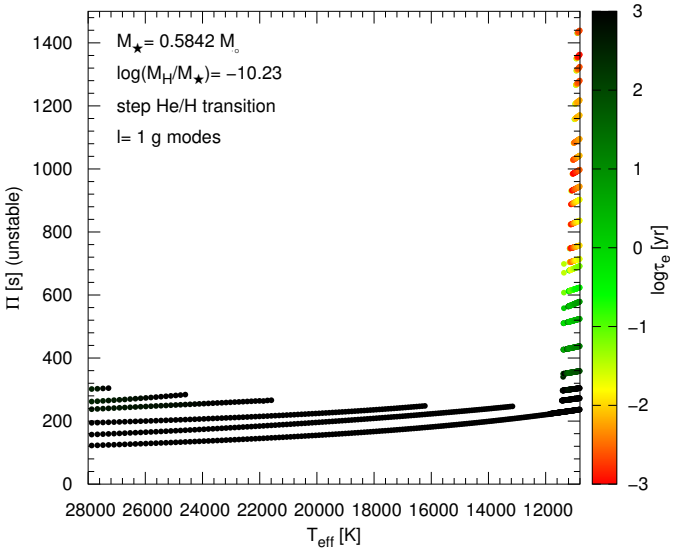

Fig. 7. Same as Fig. 5 but for $\log(M_{\rm H}/M_\star) = -10.2$. Here, a few low-order modes ($k = 1, \ldots, 6$) are *marginally* unstable apart from the unstable g modes at the ZZ Ceti's effective temperatures.

thinner H envelope: $\log(M_{\rm H}/M_\star) = -14.5$ with an abrupt H/He transition region. This is the thinnest H envelope considered in this work. Our results for this sequence indicate pulsational instability, but only for $T_{\rm eff} \lesssim 15\,000$ K. We adopt the thickness of this envelope as the lower limit for instability pulsational in warm DA WDs.

Fig. 7 displays the case of a sequence of models with the same stellar mass, $M_\star$=0.584$M_\odot$, but a thick H envelope of $\log(M_{\rm H}/M_\star) = -10.2$ having a step-like shaped H/He transition region. We find only marginal mode driving of low order g modes ($k \leq 6$) at high effective temperatures. Indeed, the e-folding time of these modes is extremely large, as emphasized by the black color for the period of these modes in Fig.7; hence they have no chance to reach observable amplitudes while the star is evolving at that stage ($\tau_{\rm e} > \tau_{\rm evol}$). On the other hand, we again obtain the unstable g modes at the ZZ Ceti stage driven by

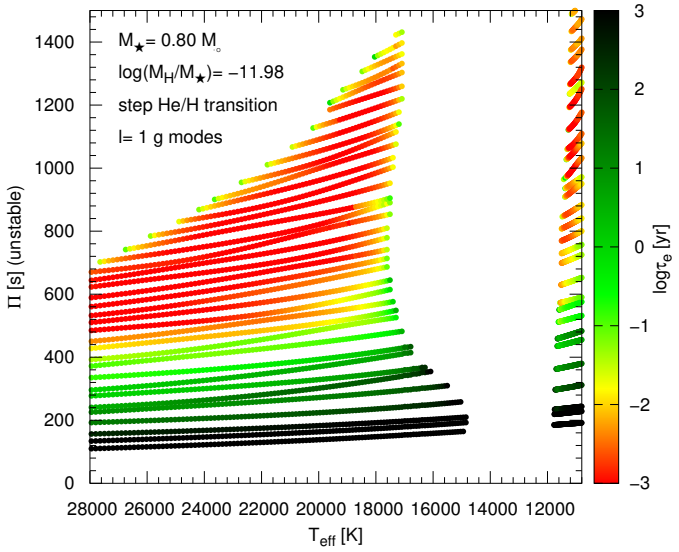

Fig. 8. Same as Fig. 5, but for $M_\star = 0.80 M_\odot$. Also for these high-mass WD models, many g modes are excited at high effective temperature.

the partial ionization zone of H via the κ mechanism. In practical terms, we can consider that there is no excitation of g modes at high effective temperatures in DA WD models with this H envelope thickness. We have repeated the stability analysis for models with the same thickness of the H envelope but with the H/He transition modeled by diffusion. Again, we do not find excitation of g modes at high effective temperatures. We conclude that this value of $M_{\rm H}/M_\star$ constitutes an upper limit for the H envelope thickness, in such a way that for thicker H envelopes there is no mode driving at high effective temperatures, even in the case in which the H/He transition is characterized by a quasi discontinuous form (step-like shape).

Finally, we have examined the case of a more massive DA WD model sequence, characterized by $M_\star$=0.80$M_\odot$ and $\log(M_{\rm H}/M_\star) = -12$. The results of our stability analysis for the case of an abrupt H/He transition is illustrated in Fig. 8. Visibly, for this stellar mass there is also excitation in many g modes for models at high effective temperatures. We also find the instability of g modes in the phase of the ZZ Ceti stars. As in the cases analyzed above, we do not find excitation of modes at high effective temperatures when the H/He chemical transition is the result of element diffusion (not shown).

5. Summary and conclusions

The existence of a new class of pulsating DA WDs hotter than ZZ Ceti stars (warm DAV WDs) was suggested long time ago by Winget et al. (1982b), who reported the occurrence of g-mode pulsational instability due to κ mechanism acting in the partial ionization zone of He below the H envelope in models of DA WDs with very thin H envelopes ($M_{\rm H}/M_\star \lesssim 10^{-10}$), for effective temperatures of $\sim 19\,000$ K. However, to date, no such warm DAV WDs have been found, despite the large number of pulsating WDs of different types discovered in the last decade both from ground based and space observational surveys. The discovery of warm DAV WDs would constitute a clear demonstration of the existence of DA WDs with very low H content, thus shedding light on the evolutionary processes that lead to WD formation in general, particularly the occurrence of late thermal pulses, the most viable scenario to form WDs with H content lower than $10^{-7} M_\odot$. The existence of such WDs cannot be discarded despite

the fact that no warm DAV WD has been observed; on the contrary, different pieces of theoretical and observational evidence suggest that a fraction of WDs should be formed with a range of very low H content.

Our paper has been conducted with the aim of exploring the impact of element diffusion on the stability pulsational properties of warm DAV WDs. We concentrated on full WD evolutionary sequences of masses 0.80 and 0.58 $M_{\odot}$ with H content in the range $M_{\rm H} \sim 10^{-10} - 10^{-14} M_{\star}$, appropriate for the study of pulsational instability of warm DAV WDs. To this end, we have used a new full-implicit treatment for time-dependent element diffusion, that maintains the sum of the chemical abundances almost constant over large time integrations. This treatment allows us to model the evolution of the outer layer chemical distribution in WDs emerging from VLTP episodes with very low H content in a realistic way, and constitutes a substantial improvement over the semi-implicit treatment considered previously in LPCODE. Initial models were extracted from progenitor star models that were evolved from the ZAMS, to the thermally-pulsing AGB phase, and through the VLTP occurring at the beginning of the cooling branch, Miller Bertolami & Althaus (2006). We find that as WD evolution proceeds, traces of H surviving the VLTP float to the surface, eventually forming thin (and increasing) pure H envelopes and rather extended H/He transition zones.

We have conducted a search for pulsating warm DA WDs among the stars observed by TESS. We have found that 36 DA WD stars with effective temperatures in the range [17 500K – 22 500 K] have been observed with TESS and we have analyzed them to search for any signs of pulsation. After examining their amplitude spectra, we conclude that none of the 36 warm DA WD stars observed by TESS show any significant frequency above the 5σ threshold. Hence, our search gives null results for pulsating warm DA WDs currently observed by TESS up to the Nyquist frequency at 4200 μHz.

Non-adiabatic pulsations of our warm DAV WD models were computed in the effective temperature range of 30 000 – 10 000 K. The driving mechanism that can excite pulsations in DA WDs in this regime is the κ mechanism due to opacity bumps resulting either from He ionization zone below the H envelope, or the H ionization zone, or both (see the pioneer works by Dolez & Vauclair 1981; Dziembowski & Koester 1981; Winget et al. 1982b). The stability analysis carried out in this work was focused on $\ell = 1$ g modes with periods in the range 50 – 1500 s. Two possibilities were considered regarding the shape of the H/He chemical interface. On the one hand, we considered this chemical transition as resulting from time-dependent element diffusion. In this case, the transition is smooth and wide. On the other hand, we assumed that this transition is extremely narrow and abrupt. Our nonadiabatic results indicate that, in order to have pulsational instability due to the κ mechanism acting at the partial ionization zone of He, it is necessary that the H/He chemical transition region be very narrow and abrupt (see Figs. 4 and 5). Our computations indicate also that the thickest H envelope for which this kind of mode excitation happens is $\log(M_{\rm H}/M_{\star}) \sim -10$, and the thinnest one is $\log(M_{\rm H}/M_{\star}) \sim -14.5$. On the other hand, if the chemical transition is smooth and extended as element diffusion predicts (see Figs. 2 and 3), then there is no excitation of modes at higher effective temperatures than those characteristic of ZZ Ceti stars, irrespective of the thickness of the H envelope.

We conclude that, assuming that DA WDs with very low H content exist, the non-detection of warm DAVs could be attributed to the fact that element diffusion produces a smooth and extended H/He interface, which inhibits the excitation of g modes due to the partial ionization of the He at effective temperatures larger than those typical of ZZ Ceti stars. In this sense, our findings could be considered as an indirect proof that element diffusion indeed operates in the interiors of WDs. However, regarding TESS, it cannot be discarded that the lack of pulsations detected in the TESS data could be attributed to that few or none of the warm DAs observed with TESS may have very thin H envelopes, or because pulsations could be below the significance thresholds, either because of low intrinsic amplitudes or high significance thresholds.

Acknowledgements. This paper includes data collected with the TESS mission, obtained from the MAST data archive at the Space Telescope Science Institute (STScI). Funding for the TESS mission is provided by the NASA Explorer Program. STScI is operated by the Association of Universities for Research in Astronomy, Inc., under NASA contract NAS 5–26555. Part of this work was supported by AGENCIA through the Programa de Modernización Tecnológica BID 1728/OC-AR, by the PIP 112-200801-00940 grant from CONICET, by MINECO grant AYA2014-59084-P, by grant G149 from University of La Plata, and by the AGAUR. M. U. acknowledges financial support from CONICYT Doctorado Nacional No. 21190886. This research has made use of NASA Astrophysics Data System.

References

Althaus, L. G., Camisassa, M. E., Miller Bertolami, M. M., Córsico, A. H., & García-Berro, E. 2015, A&A, 576, A9
Althaus, L. G., Córsico, A. H., Bischoff-Kim, A., et al. 2010a, ApJ, 717, 897
Althaus, L. G., Córsico, A. H., Isern, J., & García-Berro, E. 2010b, A&A Rev., 18, 471
Althaus, L. G., Miller Bertolami, M. M., & Córsico, A. H. 2013, A&A, 557, A19
Althaus, L. G., Miller Bertolami, M. M., Córsico, A. H., García-Berro, E., & Gil-Pons, P. 2005a, A&A, 440, L1
Althaus, L. G., Serenelli, A. M., Córsico, A. H., & Montgomery, M. H. 2003, A&A, 404, 593
Althaus, L. G., Serenelli, A. M., Panei, J. A., et al. 2005b, A&A, 435, 631
Baran, A. S., Koen, C., & Pokrzywka, B. 2015, MNRAS, 448, L16
Blöcker, T. 2001, Ap&SS, 275, 1
Bond, H. E., Bergeron, P., & Bédard, A. 2017, ApJ, 848, 16
Borucki, W. J., Koch, D., Basri, G., et al. 2010, Science, 327, 977
Castanheira, B. G. & Kepler, S. O. 2009, MNRAS, 396, 1709
Castanheira, B. G., Kepler, S. O., Kleinman, S. J., Nitta, A., & Fraga, L. 2013, MNRAS, 430, 50
Castanheira, B. G., Kepler, S. O., Mullally, F., et al. 2006, A&A, 450, 227
Córsico, A. H., Althaus, L. G., & Miller Bertolami, M. M. 2006, A&A, 458, 259
Córsico, A. H., Althaus, L. G., Miller Bertolami, M. M., et al. 2012, MNRAS, 424, 2792
Dolez, N. & Vauclair, G. 1981, A&A, 102, 375
Dufour, P., Blouin, S., Coutu, S., et al. 2017, in Astronomical Society of the Pacific Conference Series, Vol. 509, 20th European White Dwarf Workshop, ed. P.-E. Tremblay, B. Gaensicke, & T. Marsh, 3
Dziembowski, W. & Koester, D. 1981, A&A, 97, 16
Fontaine, G. & Brassard, P. 2008, PASP, 120, 1043
Fontaine, G. & Wesemael, F. 1987, in IAU Colloq. 95: Second Conference on Faint Blue Stars, ed. A. G. D. Philip, D. S. Hayes, & J. W. Liebert, 319–326
García-Berro, E., Torres, S., Althaus, L. G., et al. 2010, Nature, 465, 194
Gentile Fusillo, N. P., Tremblay, P.-E., Gänsicke, B. T., et al. 2019, MNRAS, 482, 4570
Henyey, L. G., Forbes, J. E., & Gould, N. L. 1964, ApJ, 139, 306
Hermes, J. J., Gänsicke, B. T., Kawaler, S. D., et al. 2017, ApJS, 232, 23
Hermes, J. J., Montgomery, M. H., Winget, D. E., et al. 2012, ApJl, 750, L28
Herwig, F., Blöcker, T., Langer, N., & Driebe, T. 1999, A&A, 349, L5
Howell, S. B., Sobeck, C., Haas, M., et al. 2014, PASP, 126, 398
Iben, Jr., I. & MacDonald, J. 1985, ApJ, 296, 540
Iben, Jr., I. & MacDonald, J. 1995, in Lecture Notes in Physics, Berlin Springer Verlag, Vol. 443, White Dwarfs, ed. D. Koester & K. Werner, 48
Jenkins, J. M., Twicken, J. D., McCauliff, S., et al. 2016, in Proc. SPIE, Vol. 9913, Software and Cyberinfrastructure for Astronomy IV, 99133E
Kepler, S. O., Pelisoli, I., Koester, D., et al. 2016, MNRAS, 455, 3413
—. 2019, MNRAS
Kepler, S. O. & Romero, A. D. 2017, in European Physical Journal Web of Conferences, Vol. 152, European Physical Journal Web of Conferences, 01011
Kleinman, S. J., Kepler, S. O., Koester, D., et al. 2013, ApJs, 204, 5
Kurtz, D. W., Shibahashi, H., Dhillon, V. S., Marsh, T. R., & Littlefair, S. P. 2008, MNRAS, 389, 1771
Kurtz, D. W., Shibahashi, H., Dhillon, V. S., et al. 2013, MNRAS, 432, 1632

Landolt, A. U. 1968, ApJ, 153, 151
Maxted, P. F. L., Serenelli, A. M., Miglio, A., et al. 2013, nature, 498, 463
McGraw, J. T., Starrfield, S. G., Liebert, J., & Green, R. 1979, in IAU Colloq. 53: White Dwarfs and Variable Degenerate Stars, ed. H. M. van Horn, V. Weidemann, & M. P. Savedoff, 377–381
Miller Bertolami, M. M. 2016, A&A, 588, A25
Miller Bertolami, M. M. & Althaus, L. G. 2006, A&A, 454, 845
Miller Bertolami, M. M., Althaus, L. G., & Córsico, A. H. 2017, in Astronomical Society of the Pacific Conference Series, Vol. 509, 20th European White Dwarf Workshop, ed. P.-E. Tremblay, B. Gaensicke, & T. Marsh, 435
Miller Bertolami, M. M., Althaus, L. G., Unglaub, K., & Weiss, A. 2008, A&A, 491, 253
Miller Bertolami, M. M., Rohrmann, R. D., Granada, A., & Althaus, L. G. 2011, ApJ, 743, L33
Mukadam, A. S., Mullally, F., Nather, R. E., et al. 2004, ApJ, 607, 982
Mullally, F., Thompson, S. E., Castanheira, B. G., et al. 2005, ApJ, 625, 966
Nitta, A., Kleinman, S. J., Krzesinski, J., et al. 2009, ApJ, 690, 560
Paquette, C., Pelletier, C., Fontaine, G., & Michaud, G. 1986, ApJS, 61, 177
Renedo, I., Althaus, L. G., Miller Bertolami, M. M., et al. 2010, ApJ, 717, 183
Ricker, G. R., Winn, J. N., Vanderspek, R., et al. 2014, in Proc. SPIE, Vol. 9143, Space Telescopes and Instrumentation 2014: Optical, Infrared, and Millimeter Wave, 914320
Romero, A. D., Córsico, A. H., Althaus, L. G., et al. 2012, MNRAS, 420, 1462
Romero, A. D., Kepler, S. O., Joyce, S. R. G., Lauffer, G. R., & Córsico, A. H. 2019, MNRAS, 484, 2711
Shibahashi, H. 2005, in EAS Publications Series, Vol. 17, EAS Publications Series, ed. G. Alecian, O. Richard, & S. Vauclair, 143–148
Shibahashi, H. 2007, in American Institute of Physics Conference Series, Vol. 948, Unsolved Problems in Stellar Physics: A Conference in Honor of Douglas Gough, ed. R. J. Stancliffe, G. Houdek, R. G. Martin, & C. A. Tout, 35–42
Tremblay, P.-E. & Bergeron, P. 2008, ApJ, 672, 1144
Voss, B., Koester, D., Østensen, R., et al. 2007, in Astronomical Society of the Pacific Conference Series, Vol. 372, 15th European Workshop on White Dwarfs, ed. R. Napiwotzki & M. R. Burleigh, 583
Wachlin, F. C., Miller Bertolami, M. M., & Althaus, L. G. 2011, A&A, 533, A139
Winget, D. E. 1982, PhD thesis, THE UNIVERSITY OF ROCHESTER.
Winget, D. E. & Kepler, S. O. 2008, ARA&A, 46, 157
Winget, D. E., Robinson, E. L., Nather, R. D., & Fontaine, G. 1982a, ApJ, 262, L11
Winget, D. E., van Horn, H. M., Tassoul, M., et al. 1982b, ApJ, 252, L65
York, D. G., Adelman, J., Anderson, Jr., J. E., et al. 2000, AJ, 120, 1579

Appendix A: A sample of warm DA WDs from TESS

Here, we show the Fourier Transforms of our sample of 36 warm DA WDs observed with TESS. Table A.1 lists the complete sample of stars including the spectral types, effective temperatures and gravities (taken from the MWDD Catalog), along with the magnitudes, observed sector and number of observation points from TESS, and the threshold (significance level as 5σ) and temporal resolution after computing the Fourier Transform. In Figs. A.1 to A.6 we depict the Fourier Transforms of the stars listed in table A.1. As can be seen, most of the analyzed stars do not exhibit signals of genuine variability, since the peaks seen in some stars at very low frequencies that are above 5σ threshold are of instrumental origin. The only exception is the star TIC 439917321. This is a member of a binary system, which includes WD+dM (dwarf M), with a period of 12.98 hours. In the FT of TIC 439917321, the peaks f_1, f_2 and f_3 (see Table A.2) are signature of binarity. The threshold is equal to 4σ = 1.5546478000000001 and 5σ = 1.94330975. After extraction of the peaks that are originated by binarity, the new threshold does not improve, and results almost with the same value: 4σ = 1.5544 and 5σ = 1.9432. The potential candidates for oscillation frequencies can be the peaks f_4 and f_5, but their amplitudes are below 4σ. With this analysis, we can conclude that TIC 439917321 is not a pulsating star.

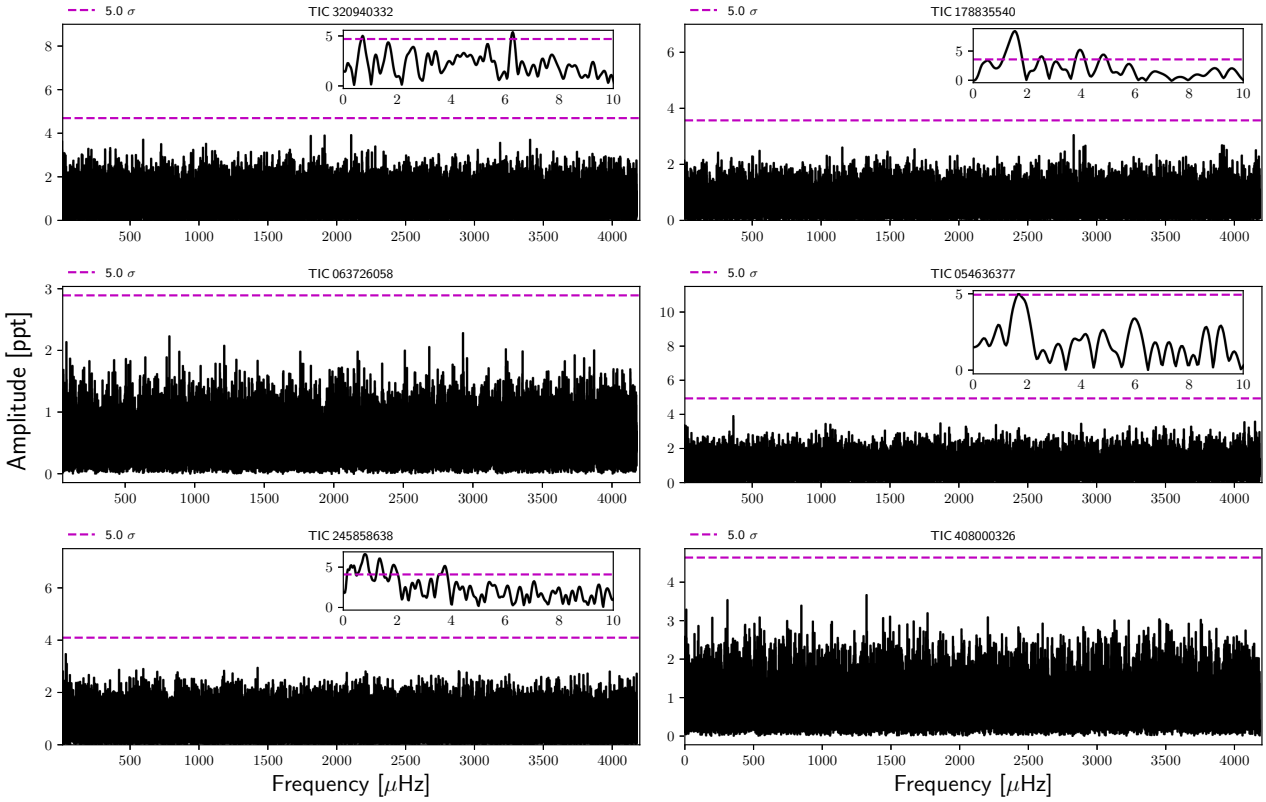

Fig. A.1. The amplitude spectra of warm DA WDs. The blue dashed horizontal line indicates the significance level. The inset is a blow-up of the amplitude spectra at the low-frequency regime.

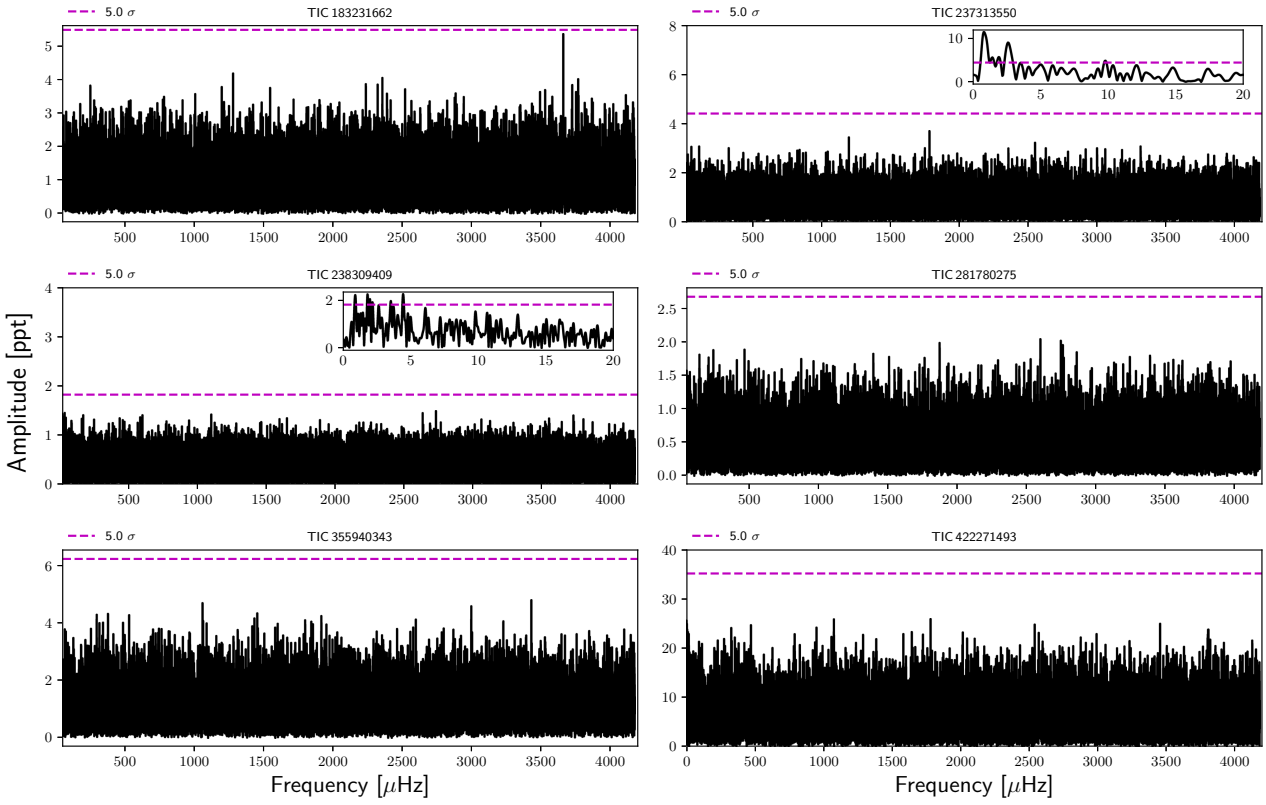

Fig. A.2. The amplitude spectra of warm DA WDs (cont.).

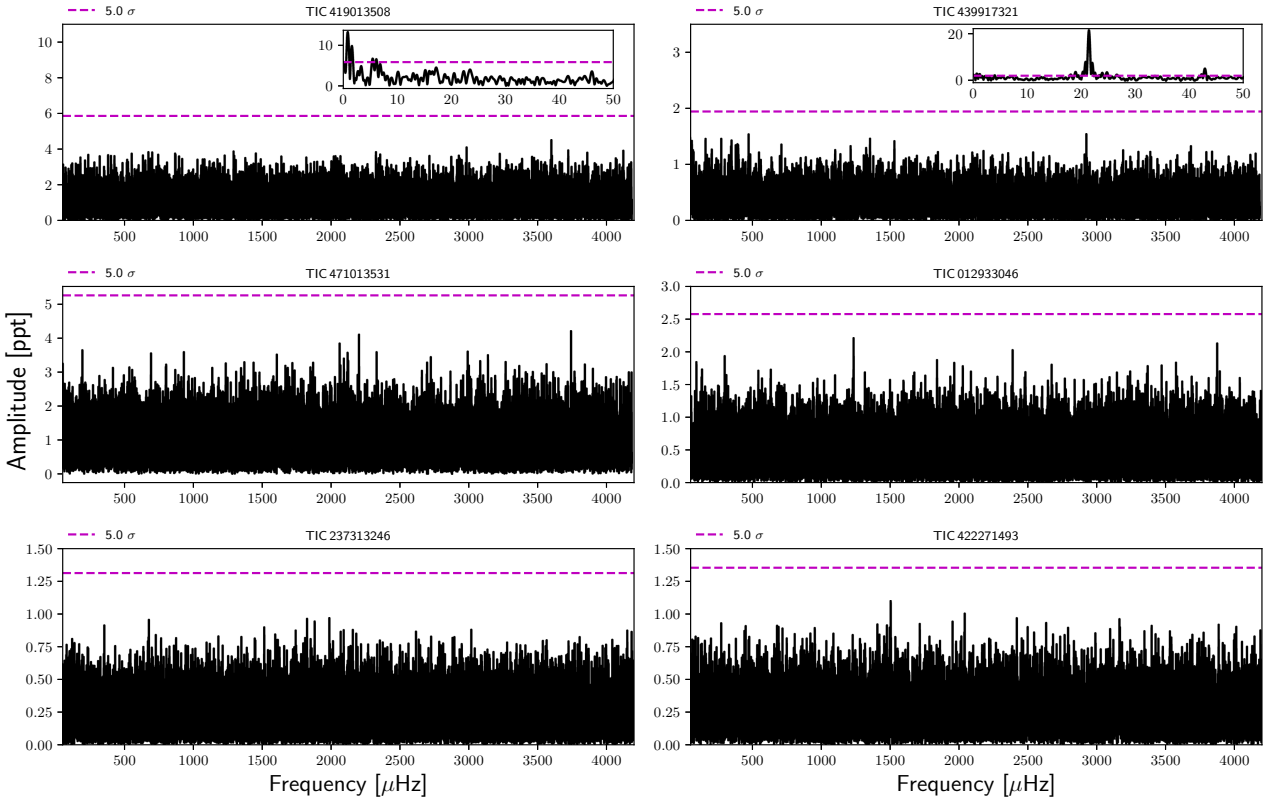

Fig. A.3. The amplitude spectra of warm DA WDs (cont.).

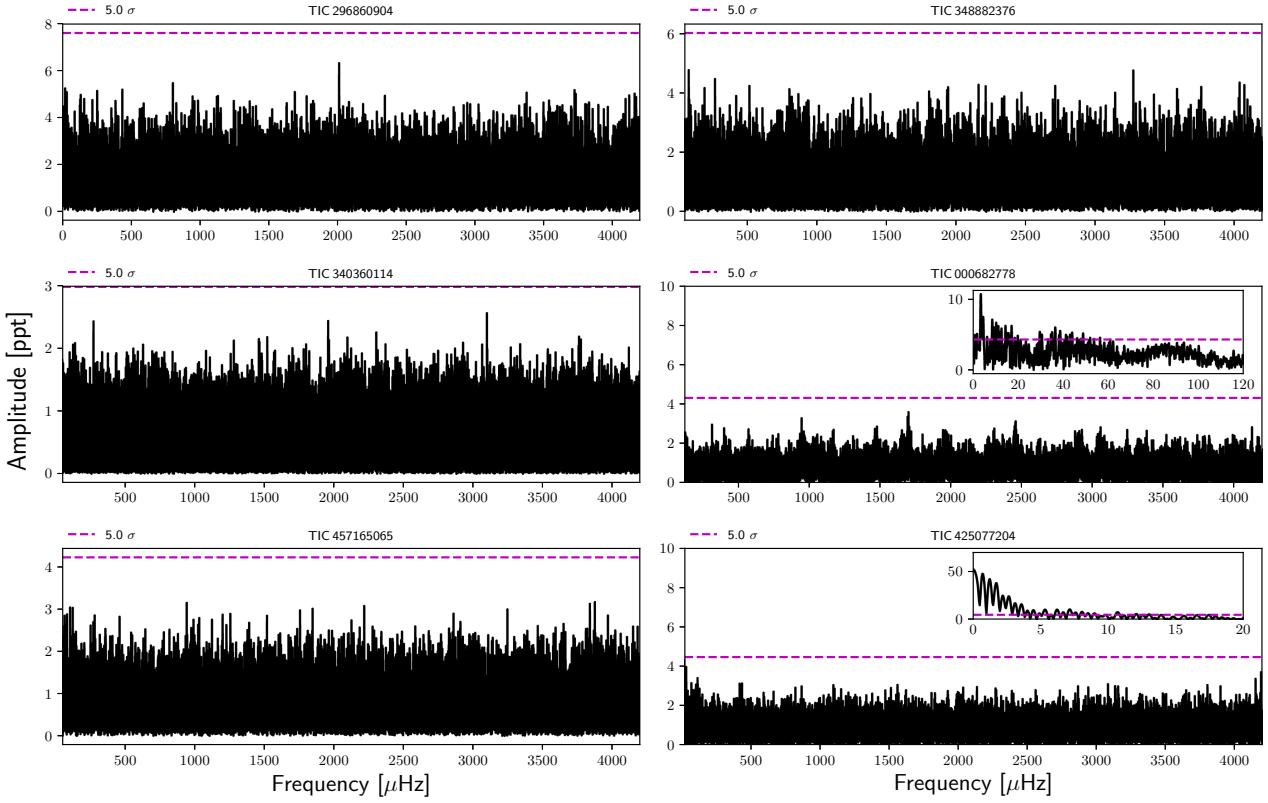

Fig. A.4. The amplitude spectra of warm DA WDs (cont.).

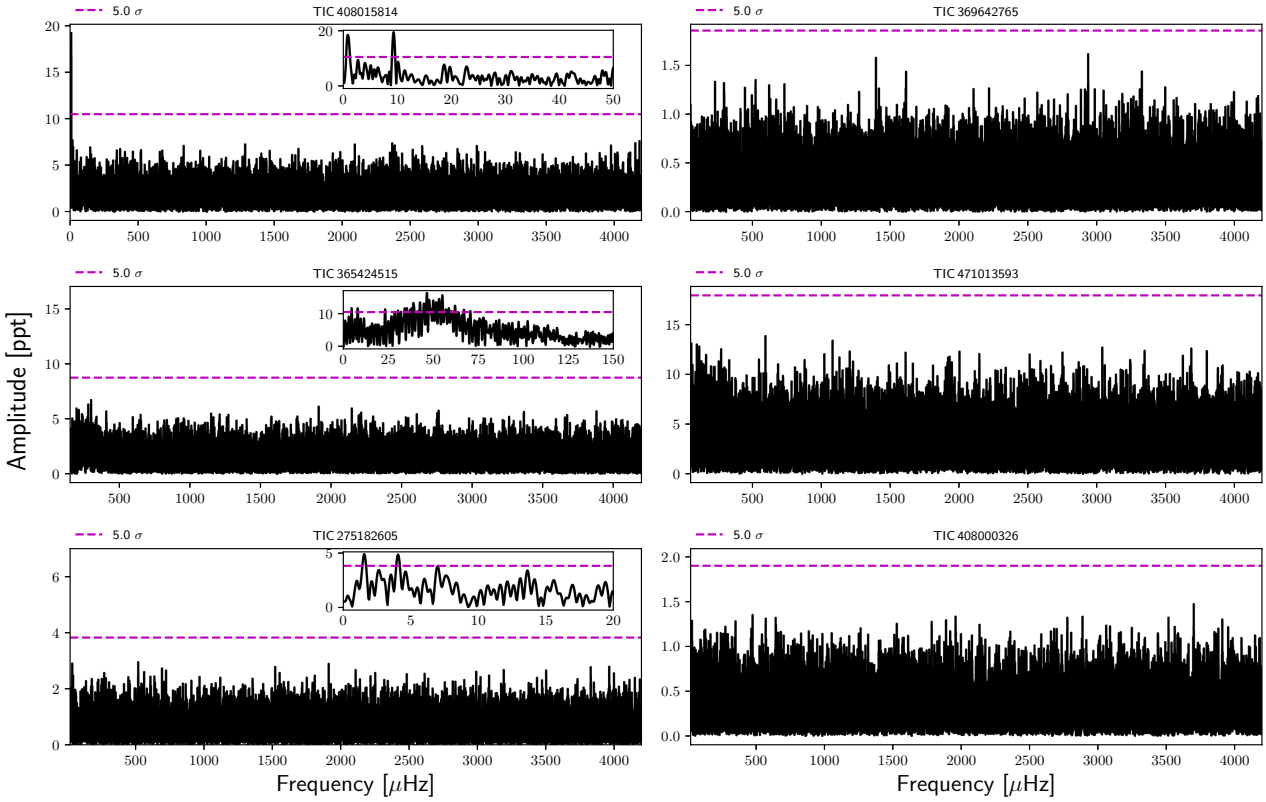

Fig. A.5. The amplitude spectra of warm DA WDs (cont.).

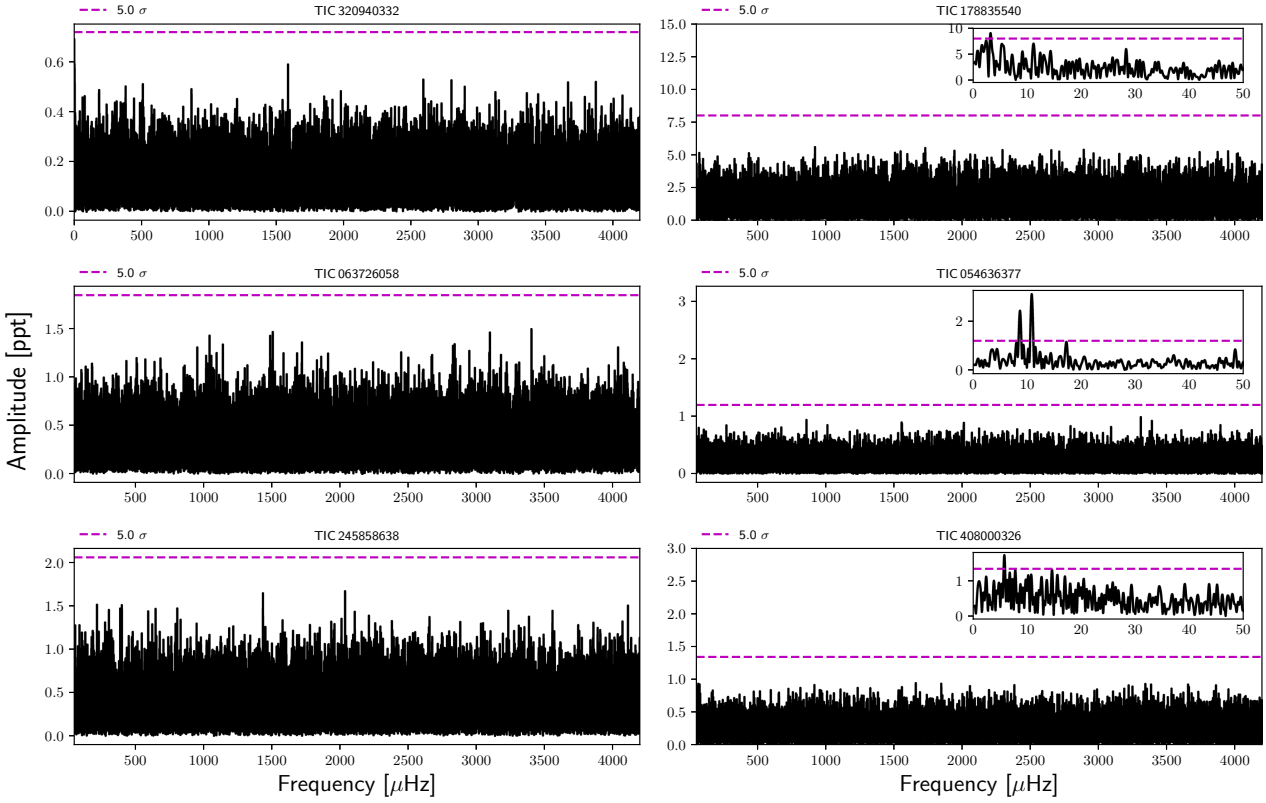

Fig. A.6. The amplitude spectra of warm DA WDs (cont.).

Table A.1. The list of our complete set of 36 warm DA WD targets including 3 different sets of information along with their names (columns 1 and 2). The first set consists of the fundamental parameters of targets from the MWDD Catalog (columns 3, 4, and 5). The second set of parameters comes from TESS mission including magnitudes, observed sector and number of observation points (columns 6, 7 and 8). Finally, the third set consists in the threshold (significance level as 5σ) and temporal resolution as $1/T$, T being the length of the data (columns 9 and 10), after Fourier transform. Stars marked with and asterisk (*) are not included in our analysis because the data of sector 10 has not been released yet.

TIC	Name	S. Type	$T_{\rm eff}$ [K]	$\log g$ [cm/s^2]	$T_{\rm mag}$	Obs. Sector	N. Points	Threshold [ppt]	Resolution [μHz]
238309409	BPM18764	DA	21970.0	7.82	14.71	7−8−9	45660	1.821	0.15
439917321	PSOJ030607	DA+M	19193.0	7.9	14.13	4	15780	1.943	0.44
001354950	HE0452−3444	DA2.5	21810.0	7.887	18.72	5	17875	4.936	0.44
007598451	HE0414−4039	DA2.4	21664.0	8.091	16.39	4−5	33671	4.693	0.22
101100431	HE0348−4445	DA	19951.0	8.069	18.83	3−4	29246	4.095	0.23
237313550	HE2251−6218	DA	18033.0	7.827	18.07	1	18104	4.414	0.42
355940343	WD0850−617	DA	21840.0	7.99	13.41	9−10(*)	16201	28.171	0.47
009143444	WD2322−181	DA	21862.0	8.009	10.29	2	18317	3.569	0.42
123370437	GD1442	DA	17810.0	7.95	17.56	3	13452	4.639	0.57
419013508	GD765	DA	18335.0	7.821	18.19	3	13452	4.688	0.57
047481377	WD1020−207	DA	18491.0	7.86	15.29	9	15602	2.892	0.48
281780275	WD0048−544	DA	17870.0	7.976	15.21	2	18316	2.676	0.42
183231662	MCT2345−3940	DA	19197.0	7.866	15.43	2	18316	5.489	0.42
287976476	BPM5102	DA	18180.0	7.87	16.79	6−10(*)	14825	6.232	0.53
471013531	GD1352	DA	19901.0	7.677	15.58	3	13452	5.262	0.57
012933046	WD 2259−267	DA	20050.0	8.03	13.71	2	18317	2.577	0.42
237313246	WD 2251−634	DA	20340.0	7.95	14.27	1	18103	1.313	0.41
422271493	WD 1049−158	DA	18085.0	8.321	13.87	9	13452	1.354	0.48
296860904	WD 1031−147	DA	22119.0	7.597	17.83	9	15602	7.601	0.48
348882376	WD 0951−155	DA	18590.0	8.01	0.0	8	13420	6.027	0.47
340360114	WD 0740−57	DA	21670.0	8.17	15.22	7−8−9−10(*)	45660	2.981	0.15
000682778	WD 0453−295	DA	20640.0	7.61	15.71	5	17871	4.307	0.44
457165065	WD 0341+021	DA	18117.0	7.132	16.71	5	17666	4.227	0.45
425077204	WD 0242−174	DA	20215.0	7.954	14.99	4	15793	4.460	0.45
408015814	WD 0053−090	DA	22372.0	6.147	17.62	3	18103	10.482	0.57
369642765	WD 0047−524	DA	18831.0	7.89	15.01	2	18316	1.857	0.42
365424515	HS 0309+1001	DA2.7	18786.0	7.725	16.16	4	15781	8.742	0.45
471013593	FBS 0341−008	DA	22588.0	7.617	16.18	5	18316	17.949	0.45
178876506	PG 1003−023	DA	18040.0	7.842	14.55	8	13420	3.826	0.46
275182605	PG 0933+026	DA	20987.0	7.821	14.27	8	13420	1.901	0.46
320940332	LP 426−26	DA	19211.0	7.959	13.85	1	18103	0.719	0.42
178835540	LB 564	DA	18722.0	7.893	19.33	8	13420	8.008	0.47
063726058	GD 603	DA	22160.0	8.508	15.01	2	15602	1.845	0.42
054636377	EGGR 57	DA	19440.0	7.92	13.79	7	16362	1.195	0.47
245858638	EGGR 39	DA	20799.0	8.104	14.73	5	17666	2.059	0.44
408000326	EGGR 31	DA	19637.0	7.933	14.25	5	17666	1.341	0.44

Table A.2. TIC 439917321

Peak	Frequency [μHz]	Amplitude [mma]
f_1	0.7046 ± 0.0281	3.090 ± 0.365
f_2	21.3915 ± 0.0037	21.133 ± 0.338
f_3	42.7931 ± 0.0152	5.122 ± 0.338
f_4	475.8455 ± 0.0505	1.544 ± 0.336
f_5	2921.8506 ± 0.0516	1.511 ± 0.336